Title
Development of a Dynamic Cathode Ejector Model for Solid Oxide Fuel Cell-Gas Turbine Hybrid Systems

Journal
Journal of Electrochemical Energy Conversion and Storage, 8(5)

ISSN
1550-624X

Authors
Maclay, James D
Brouwer, Jacob
Samuelsen, G Scott

Publication Date
2011-10-01

DOI
10.1115/1.4003774

Development of a Dynamic Cathode Ejector Model for Solid Oxide Fuel Cell-Gas Turbine Hybrid Systems

James D. Maclay

Jacob Brouwer[1]
e-mail: jb@nfcrc.uci.edu

G. Scott Samuelsen

Advanced Power and Energy Program,
University of California,
Irvine, CA 92617

Solid oxide fuel cell-gas turbine (SOFC-GT) hybrid systems are attractive for future power generation with ultra-low criteria pollutant and greenhouse gas emissions. One of the challenges for SOFC-GT systems is to sufficiently pre-heat incoming air before it enters the fuel cell cathode. An ejector for cathode exhaust recirculation has the benefits of reliability, low maintenance, and cost compared to either recuperators or cathode recirculation blowers, which may be also be used for air pre-heating. In this study, a dynamic Simulink model of an ejector for cathode exhaust recirculation to pre-heat incoming fuel cell air has been developed. The ejector is to be utilized within a 100 MW SOFC-GT dynamic model operating on coal syngas. A thorough theoretical development is presented. Results for the ejector were found to be in good agreement with those reported in literature. [DOI: 10.1115/1.4003774]

Keywords: SOFC-GT hybrid system, IGFC, fuel cell, gas turbine, cathode ejector, cathode recirculation, dynamic modeling

1 Introduction

The need for advanced coal based power generation has led to the concept of an integrated gasification fuel cell system (IGFC). The main power block in this system is comprised of a solid oxide fuel cell (SOFC) integrated with a gas turbine (GT) operating on coal syngas. Detailed descriptions of such an integrated hybrid cycle or of a simple-cycle solid oxide fuel cell (SOFC) operating on coal syngas have been outlined in the literature [1–4]. The main benefits of IGFC systems are that they allow operation on an abundant and cheap fuel and by using syngas in place of solid coal many of the toxic emissions associated with coal based power generation are removed. Additional benefits include very high electrical efficiencies that are possible by using a SOFC-GT hybrid system [5–14], and the separated anode and cathode flows of a fuel cell that more readily enable carbon concentration for sequestration. Finally, synergies between the SOFC and various gasifiers can be exploited to further increase overall system efficiency. One such potential synergy involves creating a higher methane content syngas, which improves the cold-gas efficiency of the gasifier. This is accomplished via internal reformation within the fuel cell, which provides a means of fuel cell cooling; reducing the excess air required for cooling and averting the associated parasitic losses.

In this study, a dynamic Simulink model of an ejector for cathode exhaust recirculation is developed. The ejector is utilized within a 100 MW SOFC-GT Simulink model operating on coal syngas shown in Fig. 1.

An ejector for cathode exhaust recirculation has the benefits of reliability and low maintenance, since it possesses no moving parts, and relatively low cost compared to a cathode recirculation blower, which may also be used in this application. However, the ejector is expected to be a larger parasitic load compared to a blower in this application. Both the ejector and blower are alternatives to costly recuperators that may also be used to pre-heat incoming compressor air before it enters the fuel cell cathode.

Some groups have developed ejector models for use in fuel cell applications [15–18]. However, these groups do not outline the theoretical development in sufficient detail, with the exception of perhaps [15]. Also, none of these groups describe the detailed theoretical development of a cathode ejector model and are instead focused upon anode ejector applications. The ejector model that is the subject of this study is used in conjunction with a SOFC-GT model developed by the National Fuel Cell Research Center (NFCRC), which has been extensively peer-reviewed and validated using dynamic experimental data from a 220 kW Siemens-Westinghouse SOFC-GT system tested at the NFCRC [19–28]. The original 220 kW model has been modified to simulate a planar SOFC and scaled up to 100 MW for IGFC applications.

2 Model Development

The cathode recirculation ejector modeled herein is grounded in the theoretical and experimental work conducted by Keenan et al. [29] and extends the theoretical work of Sun et al. [30]. The ejector model solves for pressure (P), temperature (T) and Mach number (M) at each section of the ejector geometry (A) diagrammed in Fig. 2. The ejector geometry is fixed but can be defined by the user to achieve different ejector performance characteristics.

The solution steps are calculated under the following assumptions:

(1) One-dimensional, steady state flow of an isentropic ideal gas.
(2) Primary and secondary fluids have the same molecular weight and ratio of specific heats.
(3) Primary and secondary fluids are supplied at zero velocities, i.e., stagnation conditions in states (1) and (2).

[1]Corresponding author.

Contributed by the Advanced Energy Systems Division of ASME for publication in the Journal of Fuel Cell Science and Technology. Manuscript received December 29, 2010; Final manuscript received February 2, 2011; Published online June 20, 2011. Editor: Nigel M. Sammes.

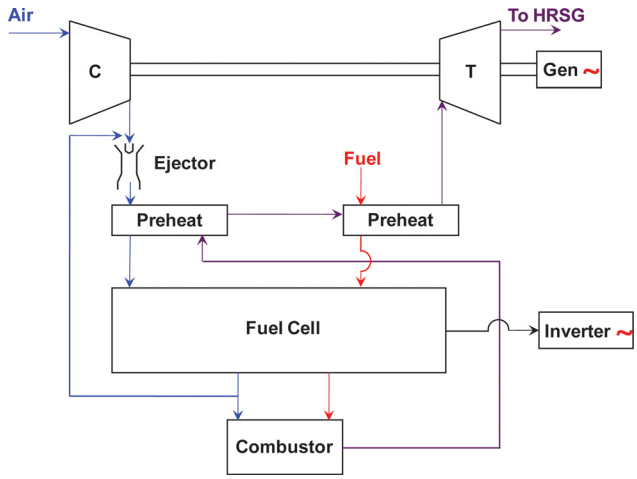

Fig. 1 Diagram of a pressurized 100 MW SOFC-GT hybrid power block utilizing an ejector for cathode recirculation

(4) At (i) the two streams meet and mixing occurs at constant pressure between (i) and (j).
(5) Transverse shock occurs at a plane between (j) and (k).
(6) Velocity at (3) is zero, i.e., stagnation conditions.
(7) Air, with a ratio of specific heats of $\gamma = 1.4$, is used for both primary and secondary fluids.

The primary fluid (denoted by the subscript 1) in this study is compressor air and the secondary fluid (denoted by the subscript 2) is cathode exhaust. A table of ejector areas A_t, A_{1i}, A_{2i} and $A_j = A_k$ is calculated for various pressure ratios P_i/P_2 using specified primary and secondary pressure and temperature stream values P_1, P_2, T_1, T_2 and ω, where ω is the entrainment ratio defined by

$$\text{Entrainment Ratio} = \omega = \frac{\dot{m}_2}{\dot{m}_1} \tag{1}$$

where $\dot{m}_1$ is the mass flow rate of the primary fluid (compressor air) and $\dot{m}_2$ is the mass flow rate of the secondary fluid (cathode exhaust). Geometry is best characterized outside of the Simulink model using methods defined by Keenan et al. [29]. The geometry necessary to create the appropriate pressure rise across the ejector P_3/P_2, accounting for pressure loss in the fuel cell and meeting the fuel cell inlet pressure design point is chosen. This is accomplished by guessing P_1 (again this is outside of the Simulink model). P_1 is the stagnation pressure value at the gas turbine compressor outlet. In the model, P_1 and gas turbine RPM will specify

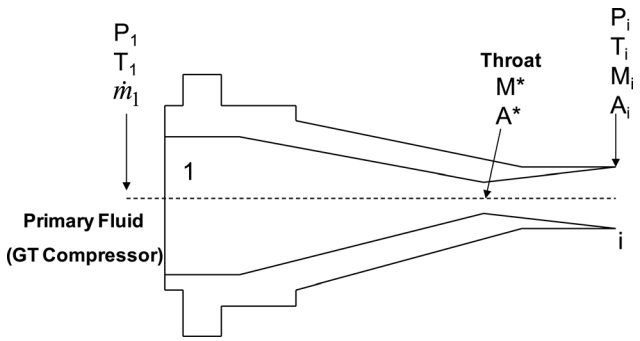

Fig. 3 Cathode ejector primary nozzle

a mass flow rate from the compressor map that defines $\dot{m}_1$ and also the stagnation temperature T_1.

For analysis of the primary nozzle (Figure 3) Table 1 is used with knowledge of ejector geometry (A/A^*, from Table 1, which is the area to critical area ratio at the throat needed for mach flow) to solve for M_{1is}. Throughout this work the subscript (s) denotes the isentropic value and (a) the actual value.

From Figure 4, it is apparent that there are two solutions for M_{1is} for a specified area ratio A/A^*. In the case that $A/A^* = 1.099$, M_{1is} is either 1.37 or 0.69. If we assume a supersonic nozzle (which is used in this model) then we chose $M_{1is} = 1.37$. Again, the value of M_{1is} comes from a look up table of supersonic Mach numbers for a given area ratio.

The actual temperature T_{1ia} out of the primary nozzle will be greater than the isentropic value T_{1is} due to inefficiencies accounted for by a nozzle efficiency term η_n in the model, a value of 90% is used; 85% is claimed to be typical of supersonic converging-diverging nozzles [30]

$$T_{1ia} = T_1\left[1 + \frac{\eta_n(\gamma - 1)}{2}M_{1is}^2\right]^{-1} \tag{2}$$

T_{2i} is known from the cathode exit conditions.

The actual Mach number M_{1ia}, accounting for efficiency loss, is calculated using

$$M_{1ia} = \sqrt{\frac{2}{\gamma - 1}\left[\left(\frac{T_1}{T_{1ia}}\right) - 1\right]} \tag{3}$$

where $M_{1ia} < M_{1is}$.

By definition nozzle efficiency does not affect P_i

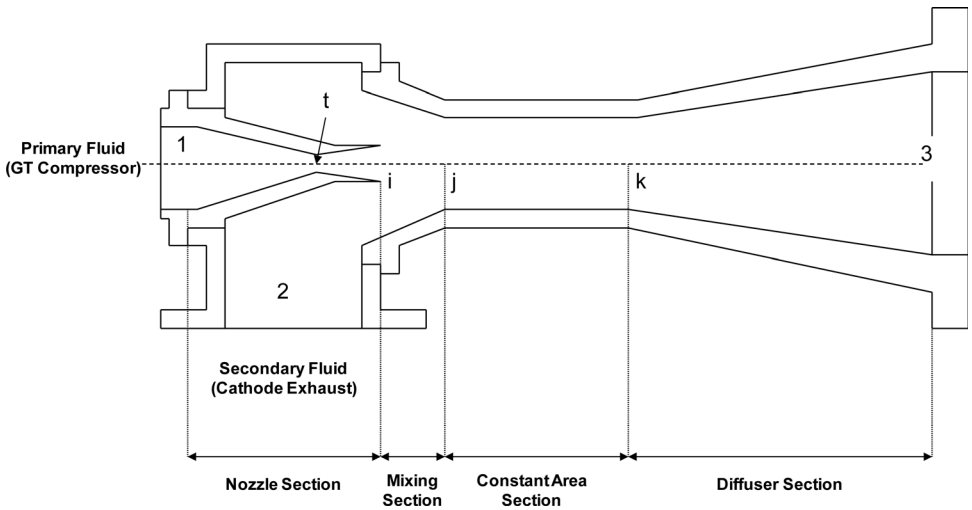

Fig. 2 Fuel cell cathode recirculation ejector

Table 1 One-dimensional isentropic compressible-flow functions for an ideal gas with constant specific heats and molar mass, $\gamma = 1.4$ (Truncated version, adapted from [31])

Ma	P/P$_1$	ρ/ρ_1	T/T$_1$	A/A*
0	1	1	1	NA
0.02	0.99972	0.9998	0.99992	28.94213
0.04	0.998881	0.9992	0.99968	14.48149
0.06	0.997484	0.998202	0.999281	9.66591
0.08	0.995533	0.996807	0.998722	7.26161
0.1	0.993031	0.995017	0.998004	5.821829
0.12	0.989985	0.992836	0.997128	4.864318
0.14	0.9864	0.990267	0.996095	4.1824
0.16	0.982285	0.987314	0.994906	3.672739
0.18	0.977647	0.983982	0.993562	3.277926
0.2	0.972497	0.980277	0.992063	2.96352
0.22	0.966845	0.976204	0.990413	2.707602
0.24	0.960703	0.971771	0.988611	2.495562
0.26	0.954085	0.966984	0.98666	2.317287
0.28	0.947002	0.961851	0.984562	2.165554
0.3	0.93947	0.95638	0.982318	2.035065

$$\eta_n = \frac{\text{Actual Kinetic Energy at Nozzle Exit}}{\text{Kinetic Energy at Nozzle Exit for Isentropic Flow from the Same Inlet State to the Same Exit Pressure}} = \frac{V_a^2/2}{V_s^2/2} = \frac{M_a^{2*}\,T_a}{M_s^{2*}\,T_s} \tag{4}$$

P_i is calculated using

$$P_i = P_1\left(1 + \frac{\gamma-1}{2}M_{1is}^2\right)^{\frac{-\gamma}{\gamma-1}} \tag{5}$$

Mixing occurs from i to j at constant pressure $P_{1i} = P_{2i} = P_j$

With knowledge of P_2 from the cathode exit conditions, M_{2i} can be solved using

$$M_{2i} = \sqrt{\frac{2}{\gamma-1}\left[\left(\frac{P_2}{P_i}\right)^{\frac{\gamma-1}{\gamma}} - 1\right]} \tag{6}$$

The entrainment ratio ω can be solved for using

$$\frac{A_{2i}}{A_{1i}} = \frac{P_1}{P_2}\left[\frac{\left(\frac{P_i}{P_1}\right)^{\frac{1}{\gamma}}\sqrt{1-\left(\frac{P_i}{P_1}\right)^{\frac{\gamma-1}{\gamma}}}}{\left(\frac{P_i}{P_2}\right)^{\frac{1}{\gamma}}\sqrt{1-\left(\frac{P_i}{P_2}\right)^{\frac{\gamma-1}{\gamma}}}}\right]\omega\sqrt{\frac{T_2}{T_1}} \tag{7}$$

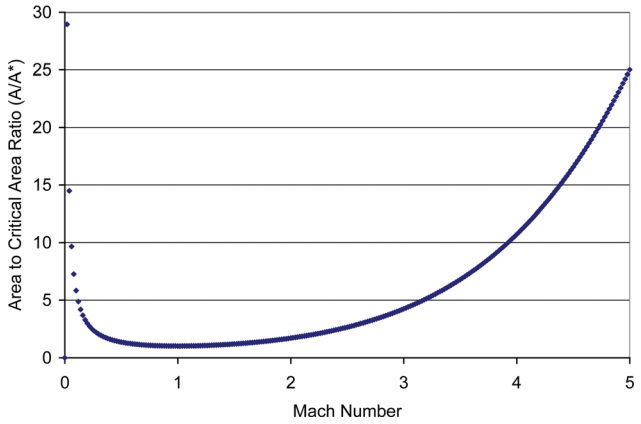

Fig. 4 Area ratio versus Mach number for isentropic flow of an ideal gas with $\gamma = 1.4$ (Air)

Rearranging we get

$$\omega = \frac{A_{2i}P_2}{A_{1i}P_1}\left[\frac{\left(\frac{P_i}{P_2}\right)^{\frac{1}{\gamma}}\sqrt{1-\left(\frac{P_i}{P_2}\right)^{\frac{\gamma-1}{\gamma}}}}{\left(\frac{P_i}{P_1}\right)^{\frac{1}{\gamma}}\sqrt{1-\left(\frac{P_i}{P_1}\right)^{\frac{\gamma-1}{\gamma}}}}\right]\sqrt{\frac{T_1}{T_2}} \tag{8}$$

The temperature at j, T_j, accounts for the mixing of streams 1 and 2 at the outlet of the constant pressure mixing section and is solved for using

$$T_j = \int\left\{\frac{\left[\left(\sum\dot{N}\int C_p dT\right) + \frac{\dot{m}V^2}{2}\right]_{IN} - \left[\left(\sum\dot{N}\int C_p dT\right) + \frac{\dot{m}V^2}{2}\right]_{OUT}}{V^* C_p^* Conc.}\right\}dT \tag{9}$$

To correct for the local speed of sound C^* which varies with temperature, the following is used

$$M^* = \frac{V}{C^*} = \frac{MC}{C^*} = \frac{M\sqrt{\gamma RT}}{\sqrt{\gamma RT^*}} = M\sqrt{\frac{T}{T^*}} \tag{10}$$

where T^* is the local temperature

$$T^* = \frac{2T_o}{\gamma+1} \tag{11}$$

and T_o is the stagnation condition. Substitution gives

$$M^* = M\sqrt{\frac{T(\gamma+1)}{2T_o}} \tag{12}$$

M_j^* is solved by substitution

$$M_j^* = \frac{M_{1ia}^* + \omega M_{2ia}^*\sqrt{\frac{T_2}{T_1}}}{\sqrt{\left(1+\omega\frac{T_2}{T_1}\right)(1+\omega)}} = \frac{M_{1ia}\sqrt{\frac{T_{1ia}(\gamma+1)}{2T_1}} + \omega M_{2i}\sqrt{\frac{T_{2i}(\gamma+1)}{2T_2}}\sqrt{\frac{T_2}{T_1}}}{\sqrt{\left(1+\omega\frac{T_2}{T_1}\right)(1+\omega)}} \tag{13}$$

$$M_j = \sqrt{\frac{2M_j^{*2}}{\gamma+1-M_j^{*2}(\gamma-1)}} \tag{14}$$

Shock is assumed to occur in the constant area section of the ejector from j to k. The equation describing a one-dimensional normal shock for an ideal gas with constant specific heats and molar mass is used to solve for M_k

$$M_k = \sqrt{\frac{\left(\frac{2}{\gamma-1}\right)+M_j^2}{\left(\frac{2}{\gamma-1}\right)\gamma M_j^2 - 1}} \tag{15}$$

The pressure rise across the shock is used to find P_k

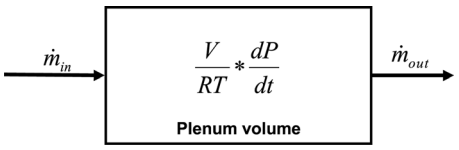

Fig. 5 Schematic of plenum volume and dynamic solution approach

$$P_k = P_j\left(\frac{M_j}{M_k}\right)\sqrt{\frac{1+\left(\frac{M_j^2(\gamma-1)}{2}\right)}{1+\left(\frac{M_k^2(\gamma-1)}{2}\right)}} \tag{16}$$

where $P_j = P_i$.

Accounting for the temperature change associated with shock in the constant area section

$$T_k = T_j\left(\frac{1+\left(\frac{M_j^2(\gamma-1)}{2}\right)}{1+\left(\frac{M_k^2(\gamma-1)}{2}\right)}\right) \tag{17}$$

Finally P_3 is determined using

$$P_3 = P_k\left[1+\left(\frac{\eta_d(\gamma-1)}{2}\right)M_k^2\right]^{\gamma/(\gamma-1)} \tag{18}$$

Where η_d is the diffuser efficiency; a value of 90% was used. 85% is claimed to be typical [30].

$P_{3a} < P_{3s}$ due to the definition of diffuser efficiency

$$\eta_d = \frac{\text{Kinetic Energy that can be Converted to Pressure Rise if the Fluid is Discharged at the Actual Exit Stagnation Pressure}}{\text{Maximum Kinetic Energy Avaialable for Converting to Pressure Rise}} = \frac{\Delta h_s}{V_1^2/2} \tag{19}$$

Using the isentropic relation $T_o/T = (P_o/P)^{(\gamma-1)/\gamma}$ which is equivalent to $T_3/T_k = (P_3/P_k)^{(\gamma-1)/\gamma}$ and by substitution into Eq. (18) we get Eq. (20), which is used to solve for the exit temperature of the ejector; an important value that will determine the effectiveness of the ejector to replace recuperation in SOFC-GT cycles

$$T_3 = T_k\left[1+\frac{\eta_d(\gamma-1)}{2}M_k^2\right] \tag{20}$$

$$T_{3a} < T_{3s}$$

In the model, P_3 and the cathode inlet pressure must be equal. In order to approach matching ejector outlet and cathode inlet pressures, ejector geometry design is iterated externally from the model. An algebraic constraint that manipulates compressor outlet pressure P_1, ultimately ensures that these pressures match exactly.

Thus far, the model development has focused upon the steady-state performance characteristics of the cathode ejector. Since a typical ejector does not have a significant volume that would allow mass storage to occur during transients, the current formulation accounts for ejector system dynamics through use of dynamic expressions for mass storage that can occur in the volumes immediately upstream and/or downstream from the ejector itself as follows. The thermodynamic state and mass flow entering or leaving the ejector system (plumbing and ejector inlet components, followed by ejector, followed by plumbing and ejector outlet components) are calculated from the flow dynamics of a plenum volume. Figure 5 schematically depicts the plenum volume considered in the current model.

The mass flow rate into the plenum volume is that entering into the ejector inlet plumbing from the immediate upstream component. The flow dynamics of the plenum volume are calculated as follows:

$$\frac{dP}{dt} = \frac{RT}{V}(\dot{m}_{in} - \dot{m}_{out}) \tag{21}$$

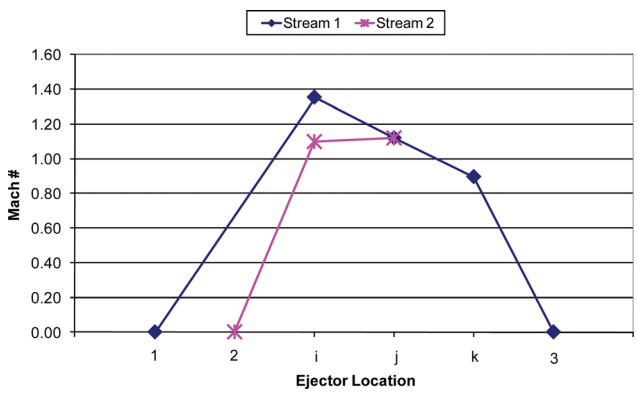

Fig. 6 Mach number versus ejector location for primary and secondary streams

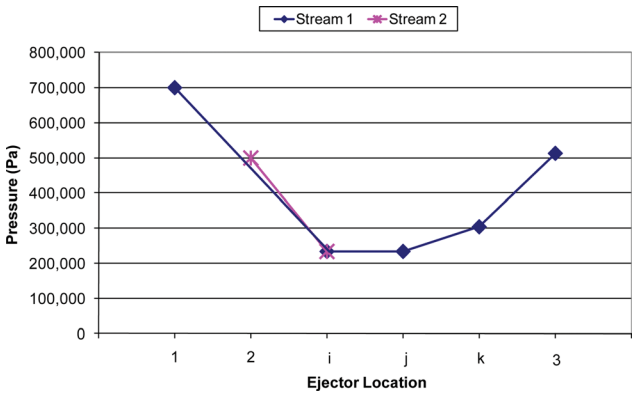

Fig. 7 Pressure versus ejector location for primary and secondary streams

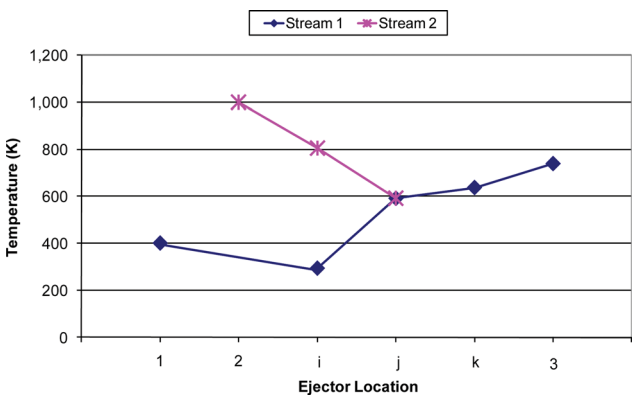

Fig. 8 Temperature versus ejector location for primary and secondary streams

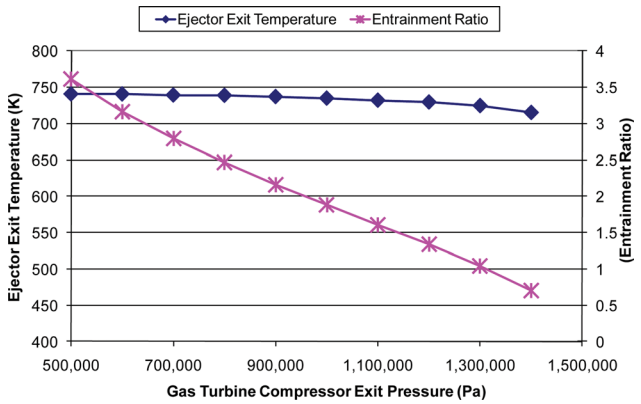

Fig. 9 Ejector exit temperature and entrainment ratio versus primary stream pressure

where P is pressure, T is temperature, V is the plenum volume before or after the ejector (m^3), and $\dot{m}_{in}$ and $\dot{m}_{out}$ are the mass flows (kg/s) in and out of the plenum volume (before or after the ejector). Note that the plenum volumes may include the volume associated with plumbing or other upstream or downstream components with sufficiently large volume to allow mass storage. Note also that a plenum volume with dynamic mass storage as described above may be inserted before and/or after the ejector as appropriate for the particular fuel cell system design one considers.

3 Results and Discussion

3.1 Ejector Model Verification. The general approach employed for the ejector model is to utilize the steady state approach developed by Keenan et al. [29], since a small volume for mass storage exists in the ejector, and to account for mass storage with dynamic input/output equations.

Figures 6, 7, and 8 show the predicted steady-state ejector model Mach number, pressure, and temperature results, respectively, at various locations in the ejector (Fig. 2). These results agree well with the literature [32–34].

Figure 9 indicates that for a fixed primary stream temperature of 400K (from the gas turbine compressor) and a fixed secondary stream temperature of 1000 K and pressure of 500 kPa (from the cathode exit) that the entrainment ratio and ejector exit temperature decrease with increasing primary stream inlet pressure; in agreement with the literature [35].

4 Conclusions

Use of an ejector for cathode exhaust recirculation in SOFC/GT systems has the benefits of reliability, low maintenance, and cost compared to either recuperators or cathode recirculation blowers. However, the dynamics of ejector operation in such applications cannot be assessed without a sufficient dynamic model. The development of a dynamic Simulink model of an ejector for cathode exhaust recirculation is presented. A thorough theoretical development is presented that may be used by other groups striving to develop and analyze the use of ejectors in fuel cell systems. Results were found to be in good agreement with those reported in literature.

Acknowledgment

The authors gratefully acknowledge the funding support of the U.S. Department of Energy (DOE) under Contract DE-AC26-04NT41817.313.01.05.036. We especially acknowledge the support and guidance of the program managers Wayne Surdoval and Travis Shultz.

References

[1] Jansen, D., van der Laag, P. C., Oudhuid, A. B. J., and Ribberink, J. S., 1994, "Prospects for Advanced Coal-Fuelled Fuel Cell Power Plants," J. Power Sources, **49**, pp. 151–165.
[2] Kuchonthara, P., Bhattacharya, S., and Tsutsumi, A., 2005, "Combination of Thermochemical Recuperative Coal Gasification Cycle and Fuel Cell for Power Generation," Fuel, **84**, pp. 1019–1021.
[3] Verma, A., Rao, A. D., and Samuelsen, G. S., 2006, "Sensitivity Analysis of a Vision 21 Coal Based Zero Emission Power Plant," J. Power Sources, **158**, pp. 417–427.
[4] Lobachyov, K., and Richter, H. J., 1996, "Combined Cycle Gas Turbine Power Plant With Coal Gasification and Solid Oxide Fuel Cell," J. Energy Resour. Tech., **118**, pp. 285–292.
[5] Winkler, W., and Lorenz, H., 2002, "The Design of Stationary and Mobile Solid Oxide Fuel Cell-Gas Turbine Systems," J. Power Sources, **105**, pp. 222–227.
[6] Winkler, W., 2006, "Fuel Cell Hybrids, Their Thermodynamics and Sustainable Development," J. Fuel Cell Sci. Tech., **3**, pp. 195–201.
[7] Winkler, W., Nehter, P., Williams, M. C., Tucker, D., and Gemmen, R., 2006, "General Fuel Cell Hybrid Synergies and Hybrid System Testing Status," J. Power Sources, **159**, pp. 656–666.
[8] Kurz, R., 2005, "Parameter Optimization on Combined Gas Turbine-Fuel Cell Power Plants," J. Fuel Cell Sci. Tech., **2**, pp. 268–273.
[9] Park, S. K., Oh, K. S., and Kim, T. S., 2007, "Analysis of the Design of a Pressurized SOFC Hybrid System Using a Fixed Gas Turbine Design," J. Power Sources, **170**, pp. 130–139.
[10] Stiller, C., Thorud, B., Seljebo, S., Mathisen, O., Karoliussen, H., and Bolland, O., 2005, "Finite-Volume Modeling and Hybrid-Cycle Performance of Planar and Tubular Solid Oxide Fuel Cells," J. Power Sources, **141**, pp. 227–240.
[11] Rao, A. D., and Samuelsen, G. S., 2002, "Analysis Strategies for Tubular Solid Oxide Fuel Cell Based Hybrid Systems," J. Eng. Gas Turbine Power, **124**, pp. 503–509.
[12] Rao, A. D., and Samuelsen, G. S., 2003, "A Thermodynamic Analysis of Tubular Solid Oxide Fuel Cell Based Hybrid Systems," J. Eng. Gas Turbine Power, **125**, pp. 59–66.
[13] Magistri, L., Bozzolo, M., Tarnowski, O., Agnew, G., and Massardo, A. F., 2007, "Design and Off-Design Analysis of a MW Hybrid System Based on Rolls-Royce Integrated Planar Solid Oxide Fuel Cells," J. Eng. Gas Turbine Power, **129**, pp. 792–797.
[14] Costamagna, P., Magistri, L., and Massardo, A. F., 2001, "Design and Part-Load Performance of a Hybrid System Based on a Solid Oxide Fuel Cell Reactor and a Micro Gas Turbine," J. Power Sources, **96**, pp. 352–368.
[15] Ferrari, M. L., Traverso, A., Magistri, L., and Massardo, A. F., 2005, "Influence of the Anodic Recirculation Transient Behavior of the SOFC Hybrid System Performance," J. Power Sources, **149**, pp. 22–32.
[16] Ferrari, M. L., Bernardi, D., and Massardo, A. F., 2006, "Design and Testing of Ejectors for High Temperature Fuel Cell Hybrid Systems," J. Fuel Cell Sci. Tech., **3**, pp. 284–291.
[17] Marsano, F., Magistri, L., and Massardo, A. F., 2004, "Ejector Performance Influence on a Solid Oxide Fuel Cell Anodic Recirculation System," J. Power Sources, **129**, pp. 216–228.
[18] Wächter, C., Lunderstädt, R., and Joos, F., 2006, "Dynamic Model of a Pressurized SOFC/Gas Turbine Hybrid Power Plant for the Development of Control Concepts," J. Fuel Cell Sci. Tech., **3**, pp. 271–279.
[19] Roberts, R. A., and Brouwer, J., 2006, "Dynamic Simulation of a 220 kW Solid Oxide Fuel-Cell-Gas-Turbine Hybrid System: Modeled Performance Compared to Measured Results," J. Fuel Cell Sci. Tech., **3**, pp. 18–25.
[20] Roberts, R. A., Brouwer, J., Junker, T., and Ghezel-Ayagh, H., 2006, "Control Design of an Atmospheric Solid Oxide Fuel Cell/Gas Turbine Hybrid System: Variable Versus Fixed Speed Gas Turbine Operation," J. Power Sources, **161**, pp. 484–491.
[21] Roberts, R., Brouwer, J., Liese, E., and Gemmen, R. S., 2006, "Dynamic Simulation of Carbonate Fuel Cell-Gas Turbine Hybrid Systems," J. Eng. Gas Turbines Power, **128**, pp. 294–301.
[22] Mueller, F., Brouwer, J., Jabbari, F., and Samuelsen, S., 2006, "Dynamic Simulation of an Integrated Solid Oxide Fuel Cell System Including Current-Based Fuel Flow Control," J. Fuel Cell Sci. Tech., **3**, pp. 144–154.
[23] Kaneko, T., Brouwer, J., and Samuelsen, G. S., 2006, "Power and Temperature Control of Fluctuating Biomass Gas Fueled Solid Oxide Fuel Cell and Micro Gas Turbine Hybrid System," J. Power Sources, **160**, pp. 316–325.
[24] Mueller, F., Jabbari, F., Brouwer, J., Roberts, R., Junker, T., and Ghezel-Ayagh, H., 2007, "Control Design for a Bottoming Solid Oxide Fuel Cell Gas Turbine Hybrid System," J. Fuel Cell Sci. Tech., **4**, pp. 221–230.
[25] Traverso, A., Massardo, A., Roberts, R. A., Brouwer, J., and Samuelsen, S., 2007, "Gas Turbine Assessment for Air Management of Pressurized SOFC/GT Hybrid Systems," J. Fuel Cell Sci. Tech., **4**, pp. 373–383.
[26] Mueller, F., Jabbari, F., Gaynor, R., and Brouwer, J., 2007, "Novel Solid Oxide Fuel Cell System Controller for Rapid Load Following," J. Power Sources, **172**, pp. 308–323.
[27] Mueller, F. Brouwer, J. Kang, S. Kim, H. S. and Min, K., 2007, "Quasi-Three-Dimensional Dynamic Model of a Proton Exchange Membrane Fuel Cell for System and Controls Development," J. Power Sources, **163**, pp. 814–829.
[28] Mueller, F., Gaynor, R., Auld, A. E., Brouwer, J., Jabbari, F., and Samuelsen, G. S., 2008, "Synergistic Integration of a Gas Turbine and Solid Oxide Fuel Cell for Improved Transient Capability," J. Power Sources, **176**, pp. 229–239.
[29] Keenan, J. H., Neumann, E. P., and Lustwerk, F., 1950, "An Investigation of Ejector Design by Analysis and Experiment," J. Appl. Mech., **72**, pp. 299–309.

[30] Sun, D. W., Eames, I. W., and Aphornratana, S., 1996, "Evaluation of a Novel Combined Ejector-Absorption Cycle- I: Computer Simulation," Int. J. Refrig., **19**, pp. 172–180.
[31] White, F. M., 2003, *Fluid Mechanics*, McGraw–Hill, New York.
[32] Chunnanond, K., and Aphornratana, S., 2004, "Ejectors: Applications in Refrigeration Technology," Renewable Sustainable Energy Rev., **8**, 129–155.
[33] Rogdakis, E. D., and Alexis, G. K., 2000, "Investigation of Ejector Design at Optimum Operating Condition," Energy Convers. Manage., **41**, pp. 1841–1849.
[34] Cengel, Y. A., and Boles, M. A., 2002, *Thermodynamics: An Engineering Approach,* McGraw–Hill, New York.
[35] Keenan, J. H., and Neumann, E. P., 1942, "A Simple Air Ejector," J. Appl. Mech., **9**, pp. A75–A81.